Ultrafast Action Potentials Mediate Kilohertz Signaling at a Central Synapse

Andreas Ritzau-Jost,[1,2,5] Igor Delvendahl,[1,2,5] Annika Rings,[1,2,5] Niklas Byczkowicz,[1,2] Harumi Harada,[3] Ryuichi Shigemoto,[3] Johannes Hirrlinger,[1,4] Jens Eilers,[1] and Stefan Hallermann[1,2,*]

[1]Carl-Ludwig-Institute for Physiology, Medical Faculty, University of Leipzig, Liebigstr. 27, 04103 Leipzig, Germany
[2]European Neuroscience Institute Göttingen, Grisebachstr. 5, 37077 Göttingen, Germany
[3]Institute of Science and Technology Austria, 3400 Klosterneuburg, Austria
[4]Department of Neurogenetics, Max-Planck-Institute for Experimental Medicine, Hermann-Rein-Strasse 3, 37075 Göttingen, Germany
[5]Co-first author
*Correspondence: hallermann@medizin.uni-leipzig.de
http://dx.doi.org/10.1016/j.neuron.2014.08.036

SUMMARY

Fast synaptic transmission is important for rapid information processing. To explore the maximal rate of neuronal signaling and to analyze the presynaptic mechanisms, we focused on the input layer of the cerebellar cortex, where exceptionally high action potential (AP) frequencies have been reported in vivo. With paired recordings between presynaptic cerebellar mossy fiber boutons and postsynaptic granule cells, we demonstrate reliable neurotransmission up to ~1 kHz. Presynaptic APs are ultrafast, with ~100 μs half-duration. Both K_{v1} and K_{v3} potassium channels mediate the fast repolarization, rapidly inactivating sodium channels ensure metabolic efficiency, and little AP broadening occurs during bursts of up to 1.5 kHz. Presynaptic $Ca_v2.1$ (P/Q-type) calcium channels open efficiently during ultrafast APs. Furthermore, a subset of synaptic vesicles is tightly coupled to Ca^{2+} channels, and vesicles are rapidly recruited to the release site. These data reveal mechanisms of presynaptic AP generation and transmitter release underlying neuronal kHz signaling.

INTRODUCTION

Information can be encoded by neural activity as the rate of action potentials (APs) (Arenz et al., 2008; London et al., 2010) and by correlations in spike timing (Rieke et al., 1997). The propagation speed of rate-coded information within a population of neurons is limited by the number of neurons and by the maximal AP frequency of each individual neuron (Rieke et al., 1997; Tchumatchenko et al., 2011). In turn, the maximal sustainable frequency of each neuron is ultimately limited by the duration of the AP (Bean, 2007; Gittis et al., 2010; Lien and Jonas, 2003; Rudy and McBain, 2001). Therefore, the AP duration is a crucial parameter limiting the speed of information processing.

Cerebellar mossy fibers represent one of the main inputs to the cerebellum and send broad-bandwidth signals to the cerebellar cortex with firing frequencies up to 1.2 kHz in vivo (Garwicz et al., 1998; Jörntell and Ekerot, 2006; Rancz et al., 2007). These high-frequency signals are conveyed to granule cells (GCs), the most abundant neurons in the entire brain. In order to connect to the large number of GCs, cerebellar mossy fibers form several collaterals and contain numerous presynaptic boutons along the myelinated axon. In addition, each cerebellar mossy fiber bouton (cMFB) contacts more than 10 GCs (Billings et al., 2014; Jakab and Hámori, 1988). Despite the high degree of divergence at cMFBs, signal transduction to the postsynaptic partners is very efficient (Chadderton et al., 2004; Jörntell and Ekerot, 2006; Rancz et al., 2007; Saviane and Silver, 2006). In a seminal study, Rancz and coworkers (2007) pioneered direct whole-cell patch-clamp recordings from cMFBs in vitro and in vivo, offering the opportunity to directly investigate the mechanisms of high-frequency signaling from single nerve terminals to a large number of postsynaptic partners.

Here, we establish paired patch-clamp recordings between cMFBs and GCs in acute cerebellar brain slices in combination with high-resolution analysis of presynaptic mechanisms. We focus on the properties of APs in cMFBs enabling kHz signaling and the mechanisms by which cMFBs can reliably release neurotransmitter to dozens of GCs. Our recordings demonstrate reliable neurotransmission at frequencies of up to ~1 kHz and reveal a surprisingly short duration of APs, which is more than 2-fold shorter than previous estimates at central neurons or axons. Furthermore, we show that efficient opening of presynaptic Ca^{2+} channels, tight coupling of vesicles to Ca^{2+} channels, and rapid vesicle recruitment sustain reliable neurotransmitter release during kHz signaling.

RESULTS

Kilohertz Transmission at Single cMFB-GC Connections

Synaptic transmission of individual cMFB-GC connections was analyzed with paired whole-cell patch-clamp recordings from cMFBs and GCs in acute cerebellar brain slices of mature mice at physiological temperatures (schematically illustrated in Figure 1A). Recordings from cMFBs were obtained with the aid of two-photon targeted patching (Margrie et al., 2003) in transgenic mice expressing yellow fluorescent protein in a subset of mossy fibers (Figure 1B; Hirrlinger et al., 2005) or with differential interference contrast microscopy in wild-type mice. For an

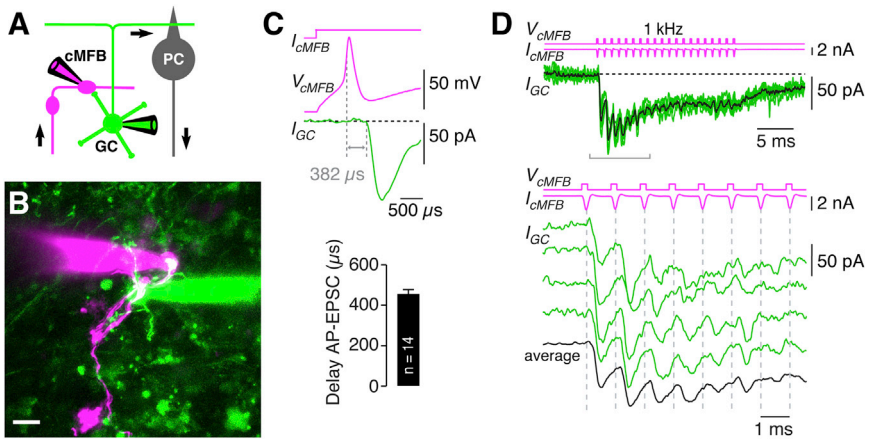

Figure 1. Kilohertz Transmission at Single cMFB-GC Connections

(A) Schematic illustration of the cellular connectivity within the cerebellar cortex. Mossy fibers (magenta) send information to the cerebellar cortex. Presynaptic cerebellar mossy fiber boutons (cMFB) transmit signals to postsynaptic granule cells (GCs, green), which excite Purkinje cells (PC, gray) via parallel fibers. Axons of Purkinje cells represent the sole output of the cerebellar cortex. Two patch-clamp pipettes illustrate the paired cMFB-GC recording configuration.

(B) Two-photon microscopic image of a paired whole-cell patch-clamp recording between a cMFB (magenta) and a GC (green) filled with the fluorescence dyes Atto 594 and Atto 488, respectively, in an acute cerebellar brain slice of a 39-day-old TgN(Thy1.2-EYFP) mouse expressing EYFP in a subset of mossy fibers (green; maximal z-projection of a stack of images over 45 µm; z-step 3 µm). Scale bar, 10 µm.

(C) Top: Example trace of a paired cMFB-GC recording with current injection (I_{cMFB}) evoking an AP in the cMFB (V_{cMFB}) and an EPSC in the postsynaptic GC (I_{GC}). The synaptic delay is indicated. Bottom: Average synaptic delay of n = 14 paired recordings (mean ± SEM).

(D) Top: Voltage clamp of a cMFB with 20 AP-like depolarizations (V_{cMFB}; 200 µs to 0 mV) at a frequency of 1 kHz evoked presynaptic action currents in the cMFB (I_{cMFB}) and EPSCs in the connected GC (four consecutive trials in green, average in black). Bottom: the first seven EPSCs on an expanded scale (cf. bracket in top panel, dashed lines are set to the peak of the action currents; see also Figure S1).

unequivocal identification of cMFBs, we determined the characteristic morphological and electrophysiological properties (see Supplemental Experimental Procedures; Figure S1; Rancz et al., 2007). Brief current injection into cMFBs evoked an AP in the cMFB and an excitatory postsynaptic current (EPSC) in a synaptically connected GC with a synaptic delay of 457 ± 20 µs (n = 14; Figure 1C). To directly analyze transmission in the kHz regime, presynaptic stimulation with 20 AP-like depolarizations (0 mV, 200 µs duration) at a frequency of 1 kHz was used to evoke presynaptic action currents in cMFBs. These presynaptic kHz bursts evoked EPSCs in GCs, consisting of a phasic EPSC, which is related to direct release onto the GC, and a tonic component, part of which is probably due to glutamate spillover from neighboring release sites onto the recorded GC (Figure 1D; DiGregorio et al., 2002). In the example shown in Figure 1D, the average phasic steady-state amplitude of the last ten EPSCs was 8.1 pA. When taking into account the previously reported reduction in EPSC amplitude due to postsynaptic depression of ~30% and the miniature EPSC amplitude of 17 pA (Hallermann et al., 2010), this corresponds to release of about one vesicle each millisecond in this cMFB-GC connection (see below for detailed analysis of the rate of vesicle recruitment). This example demonstrates that a single cMFB-GC connection can reliably transmit information during short bursts at a frequency of 1 kHz.

Ultrafast APs in cMFBs

In order to understand the mechanisms of high-frequency burst signaling, we next analyzed the properties of presynaptic APs. Upon current injection, cMFBs fired APs with durations at half-maximal amplitude of 107 ± 4 µs (n = 44; referred to as half-duration in the following; Figure 2B). To analyze APs undisturbed by a presynaptic depolarization, cMFBs and the adjacent axon were filled with a fluorescent dye (Figure 2A) and a distal part of the axon was approached with a stimulation pipette. We systematically compared APs elicited by current injection and axonal stimulation. The half-duration of APs elicited in the same cMFB was not significantly different between the two modes of AP generation (n = 10, p = 0.1, Wilcoxon signed-rank test; Figure 2C). These data demonstrate that APs of cMFBs are ultrafast with a half-duration of ~100 µs.

To gain insights into the mechanisms allowing such short AP half-duration, we analyzed which K^+ channel subtypes are responsible for AP repolarization. Focal application of the K_{v3} channel gating modifier BDS-I (3 µM; Martina et al., 2007) prolonged AP half-duration to 202 ± 14 µs (n = 11, p < 0.001, Mann-Whitney U test), whereas bath application of the K_{v1} channel blocker α-dendrotoxin (DTX, 0.2 mM) prolonged the half-duration to 265 ± 27 µs (n = 11, p < 0.001, Mann-Whitney U test; Figures 2D, 2E, and S2). The impact of K_{v3} channels could be underestimated in these experiments because of incomplete focal application of BDS-I or the fact that BDS-I only slows gating but does not block K_{v3} completely (Martina et al., 2007). However, bath application of 1 mM TEA, which blocks $K_{v1.1}$ and all K_{v3} channel subtypes (Gutman et al., 2005), did not have a stronger effect on AP half-duration than focal BDS-I application (p = 0.75; Mann-Whitney U test; Figure 2E). This finding indicates that BDS-I application was successful and that the slowing of the K_{v3} activation kinetics by BDS-I (Martina et al., 2007) corresponds to a complete K_{v3} block during the duration of our APs. Finally, application of 5 mM 4-AP, which blocks K_{v1} and K_{v3} channels, resulted in APs with half-durations of ~1 ms (n = 5, p < 0.001, Mann-Whitney U test; Figures 2D and 2E). Although we have not addressed K_{v2} and K_{v4} channels specifically, a strong contribution to the AP repolarization is unlikely, because K_{v2} channels activate slowly and contribute only to repolarization of longer APs (Liu and Bean, 2014), and K_{v4} channels have been shown to localize preferentially to somata and dendrites (Sheng et al., 1992). These data indicate that primarily K^+ channels of the K_{v1} and the K_{v3} channel families mediate the repolarization of ultrafast cMFB APs.

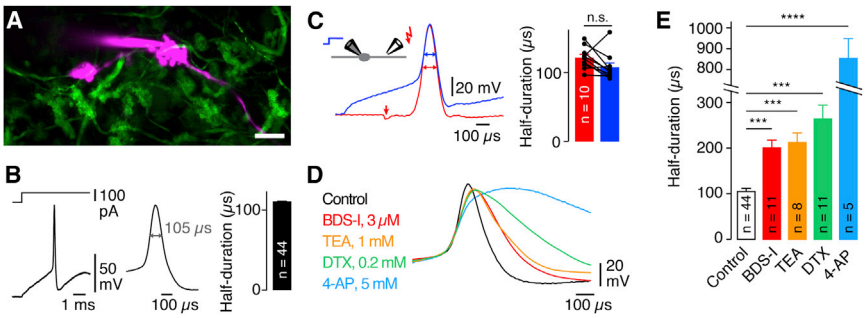

Figure 2. Ultrafast APs in cMFBs

(A) Two-photon image of a whole-cell patch-clamped cMFB and the adjacent axon (magenta; Atto 594 in the pipette solution) in an acute cerebellar brain slice of a 48-day-old TgN(Thy1.2-EYFP) mouse with EYFP-labeled mossy fibers (green; maximal z-projection of a stack of images over 20 μm; z-step 1 μm). Scale bar, 10 μm.

(B) Example of an AP recorded in a cMFB evoked by current injection. Middle: Same example on an expanded time scale (AP half-duration is indicated). Right: Average AP half-duration elicited by current injection (mean ± SEM; n refers to the number of cMFBs).

(C) Left: Comparison of APs elicited by current injection (blue) and axonal stimulation with a second pipette (red) in the same cMFB as illustrated by the color code of the inset. Example APs elicited in both ways are superimposed (arrow indicates stimulation artifact). Right: Comparison between the AP half-duration elicited by axonal stimulation (red) and current injection (blue) in the same cMFBs (mean ± SEM; connected dots represent results from the two stimulation conditions in the same cMFB).

(D) Examples of cMFB APs measured in the presence of indicated K^+ channel blockers. APs were evoked by current injection. Voltage traces are aligned to the AP threshold.

(E) Average AP half-duration after application of the indicated K^+ channel blockers (mean ± SEM). Asterisks indicate significance as described in the text (see also Figure S2).

Fast Inactivating Na^+ and Activating K^+ Channels Generate Ultrafast and Metabolically Efficient APs

We next applied an AP waveform (measured in cMFBs with axonal stimulation) as voltage command to outside-out patches from cMFBs to analyze the Na^+ and K^+ currents underlying the fast cMFB APs. The pharmacologically isolated currents had very short half-durations of 73 ± 9 μs (n = 6) and 61 ± 2 μs (n = 5; Figures 3A and 3B) for Na^+ and K^+, respectively. Metabolic efficiency was quantified as the Na^+ excess ratio, defined as the total Na^+ influx (Na^+ current integrated over the entire duration of the AP) divided by the Na^+ flux until the time of the AP peak (Figure 3C). The Na^+ excess ratio was 1.76 ± 0.12 (n = 6), which is efficient compared with APs of short duration at other preparations (Carter and Bean, 2009, 2011).

To analyze the mechanisms that generate ultrafast but metabolically efficient APs, we studied the kinetic parameters of Na^+ and K^+ currents. Step-depolarizations from −80 to 0 mV applied to outside-out patches revealed rapid Na^+ channel inactivation with a time constant of 81 ± 3 μs (n = 5; Figure 3D), which is consistent with corresponding recordings from axons of fast-spiking interneurons at room temperature, assuming a Q_{10} temperature coefficient of 2.6 (time constant ~300 μs; Hu and Jonas, 2014). Maximally activating voltage steps from −80 to +40 mV were applied to investigate the kinetics of K^+ currents at cMFBs. The activation time constant was 225 ± 24 μs (n = 12; Figure 3E), which is consistent with previous studies of rapidly activating K^+ channels (Martina et al., 2007). Thus, rapid inactivation of Na^+ and activation of K^+ channels underlie efficient cMFB APs.

In order to further dissect whether the kinetics or rather the density of Na^+ and K^+ channels cause the short half-duration of the APs, we estimated current densities from outside-out patches and performed Hodgkin-Huxley modeling based on the measured gating kinetics (Figure S3; see Supplemental Experimental Procedures). However, with the estimated Na^+ and K^+ conductance ($\bar{g}_{Na}$ = 722 and $\bar{g}_K$ = 82 pS • μm^{-2}), the model predicted a too-long half-duration (Figure S3E). To obtain the measured half-duration, a ~10-fold higher K^+ current density was required. An inhomogeneous distribution of K^+ channels could explain this finding (see Discussion). Thus, our approach of high-resolution kinetic analysis of Na^+ and K^+ currents in combination with Hodgkin-Huxley modeling provides indirect evidence for an inhomogeneous distribution of K^+ channels and indicates a high density of Na^+ channels.

Stable APs during kHz Bursts

We evoked presynaptic APs by axonal stimulation at increasing rates (250–2,000 Hz) to analyze the AP shape during high-frequency firing. cMFBs were capable of firing failure-free trains of APs at exceptionally high frequencies (Figure 4A). In the illustrated example, failure-free trains of APs were elicited at up to 1.6 kHz and had almost constant amplitude and half-duration up to 1 kHz (Figures 4A and 4B), suggesting a rapid recovery from sodium channel inactivation (Leão et al., 2005). At frequencies close to the maximal failure-free frequency, slight amplitude reduction and broadening occurred, which fully recovered within a few tens of milliseconds (Figure 4B). Interestingly, the maximal failure-free AP frequency correlated with the AP half-duration (Figure 4C). On average, failure-free frequency for 11 APs was 1.0 ± 0.1 kHz (n = 10; Figure 4D). At the frequency tested before the maximal failure-free frequency (mean 800 ± 89.8 Hz), last AP half-duration was 111 ± 2.5%, and AP amplitude 95.1 ± 1.7% of the first AP (n = 10). These data are similar to findings obtained at the calyx of Held (Wang and Kaczmarek, 1998) and at cMFBs in vivo (Rancz et al., 2007). In contrast, nerve terminals operating at lower frequencies, such as hippocampal mossy fiber boutons, exhibit pronounced AP broadening even at frequencies of 1–100 Hz (Geiger and Jonas, 2000). Thus, cMFBs can generate APs at kHz frequencies with little amplitude reduction and broadening.

Efficient Opening of Ca^{2+} Channels during cMFB APs

In order to understand the mechanisms of synaptic transmission at these frequencies, we next investigated whether the ultrafast APs in cMFBs can reliably open Ca^{2+} channels. With optimized recording conditions (see Supplemental Experimental Procedures), AP-evoked Ca^{2+} currents (Borst and Sakmann, 1998)

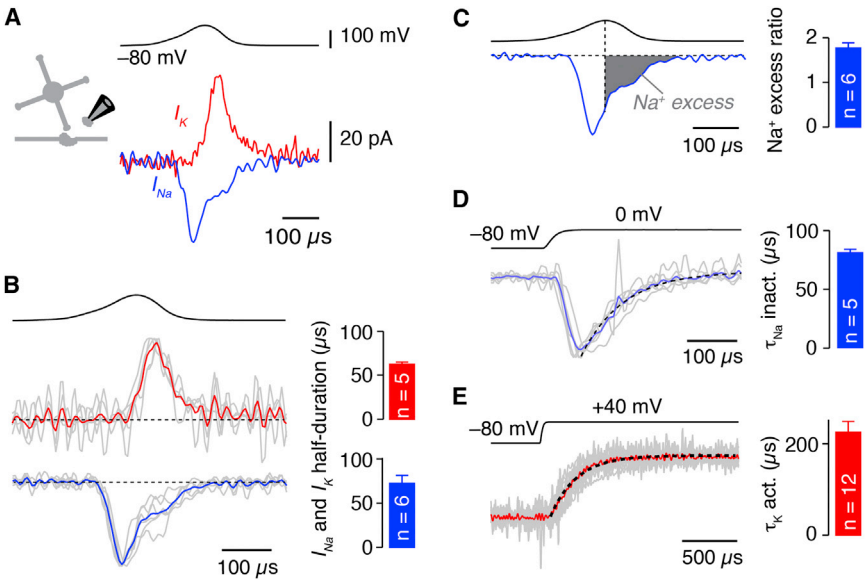

Figure 3. Fast Inactivating Na^+ and Activating K^+ Channels Generate Ultrafast and Metabolically Efficient APs

(A) Examples of pharmacologically isolated Na^+ (blue) and K^+ currents (red) in two different outside-out patches from cMFBs, elicited by a previously recorded AP voltage command (top). Traces are averages of 82 and 101 sweeps for Na^+ and K^+ currents, respectively. Inset: Schematic illustration of the recording configuration.

(B) Superposition of peak normalized AP-evoked currents (gray traces; n = 6 for Na^+, n = 5 for K^+; n represents number of outside-out patches) with the corresponding grand averages (Na^+, blue; K^+, red). Right: Average half-duration of AP-evoked Na^+ (blue) and K^+ current (red; mean ± SEM).

(C) Average AP-evoked Na^+ current. Filled gray area indicates the excess Na^+ influx following the peak of the AP. Right: Average Na^+ excess ratio calculated as total Na^+ influx divided by the Na^+ influx until the time of the AP peak (mean ± SEM).

(D) Superposition of peak normalized Na^+ currents (n = 5, gray) elicited by 3 ms depolarization from −80 mV to 0 mV with the grand average (blue) and an exponential fit to the time course of inactivation (black dashed line). Right: Average time constant of inactivation (mean ± SEM).

(E) Superposition of peak normalized K^+ currents (n = 12, gray) evoked by 3 ms depolarizations from −80 mV to +40 mV with the grand average (red) and an exponential fit to the time course of activation (black dashed line). Right: Average time constant of activation (mean ± SEM; see also Figure S3).

could be resolved having an amplitude of 543 ± 62 pA and a half-duration of 99 ± 4 µs (n = 9; Figure 5A). To determine the relative open probability of Ca^{2+} channels during an AP, Ca^{2+} currents were elicited by AP-like depolarizations of variable duration (Figure 5B). On average, 59% of the available Ca^{2+} current was recruited during an AP (Figure 5C). To understand the efficient opening during short APs, we measured the kinetics of Ca^{2+} currents in cMFBs and found rapid activation and deactivation (Figures S4A and S4B). A two-gate Hodgkin-Huxley model based on the measured activation and deactivation kinetics (Figure S4C) reproduced the AP-evoked Ca^{2+} current (Figure 5A) and predicted a relative open probability of 77% during an AP. Thus, rapid kinetics of presynaptic Ca^{2+} channels can explain the efficient opening of Ca^{2+} channels during short APs at cMFBs.

$Ca_V2.1$ Ca^{2+} Channels at Active Zones of cMFBs

To identify the molecular identity of the presynaptic Ca^{2+} channels at cMFBs, whole-cell Ca^{2+} currents were recorded during application of specific Ca^{2+} channel blockers (Figure 6A). ω-Agatoxin (0.5 µM), which selectively blocks $Ca_V2.1$ (P/Q-type) Ca^{2+} channels, inhibited 70.8% ± 4.3% (n = 10) of the Ca^{2+} current. In contrast, 1 µM ω-Conotoxin, which blocks $Ca_V2.2$ (N-type) Ca^{2+} channels, and 0.5 µM SNX-482, which blocks $Ca_V2.3$ (R-type) Ca^{2+} channels, inhibited only 15.5% ± 2.8% (n = 11) and 11.9% ± 1.8% (n = 5) of the Ca^{2+} current, respectively (Figure 6B). Thus, $Ca_V2.1$ Ca^{2+} channels mediate the majority of the Ca^{2+} current at cMFBs. To investigate whether these channels are localized at the active zone, we analyzed the localization of $Ca_V2.1$ Ca^{2+} channels using pre-embedding immunogold labeling for $Ca_V2.1$ in mice (Indriati et al., 2013). Immunogold particles for $Ca_V2.1$ were often found in the presynaptic active zone of cMFBs making synapses onto granule cell dendrites (Figure 6C). The density of particles was ~50 times higher at the active zone compared with extrasynaptic membrane (Figure 6D). Consistently, freeze-fracture replica labeling of cerebellar granule cell layer also showed clustered $Ca_V2.1$ Ca^{2+} channels at putative active zones of cMFBs (Figure 6E). These data indicate that $Ca_V2.1$ Ca^{2+} channels, which are clustered at active zones, represent the majority of Ca^{2+} channels at cMFBs.

Measuring Vesicular Release Simultaneously from Presynaptic Capacitance Increase and Postsynaptic Currents

To understand how the brief Ca^{2+} influx can elicit synchronous release during kHz bursts, we next analyzed fundamental parameters of release, such as the number of release-ready vesicles, the speed of vesicle recruitment, and the vesicle to Ca^{2+} channel coupling distance. We combined two independent techniques to measure these parameters in the paired-recording configuration: presynaptic capacitance measurements and deconvolution of postsynaptic currents (Sakaba, 2006; Sun and Wu, 2001; von Gersdorff et al., 1998; Wölfel et al., 2007). Depolarizing pulses of increasing duration (0 mV; 1–100 ms) were applied to the presynaptic terminal (Figure 7A). The presynaptic Ca^{2+} current, the induced capacitance increase due to vesicle exocytosis, and the evoked postsynaptic current were measured simultaneously. Deconvolution of postsynaptic currents led to an estimate of presynaptic release rates during the pulses (Figure 7A; see Supplemental Experimental Procedures). The capacitance increase and the number of vesicles estimated by deconvolution scaled linearly for depolarizations of 1–100 ms

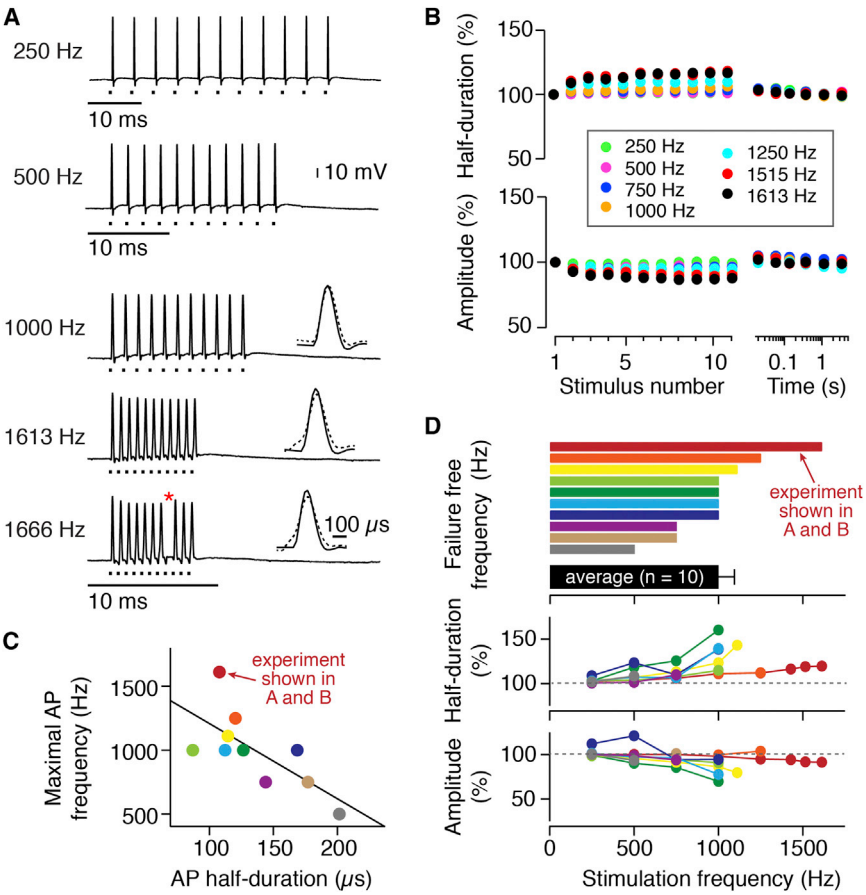

Figure 4. Stable APs during kHz Bursts

(A) Examples of APs recorded in a cMFB elicited at the indicated frequencies by axonal stimulation with an extracellular stimulation pipette (stimulation time points are indicated as dots below the traces; lowest scale bar applies to all three lowest traces). An overlay of the first (solid) and last (11th, dashed) AP is shown on the right. Note the failure after the seventh AP at 1,666 Hz (red asterisk).

(B) Time course of AP broadening and amplitude reduction of the experiment shown in (A) at the color-coded frequencies. The amplitude and half-duration of 11 APs during the train are plotted versus the stimulus number (normalized to the first AP). The properties of the APs that were elicited with increasing intervals following the train stimulation (not shown in A) are plotted versus the time after the end of the train. Note the stable half-duration and amplitude during bursts of up to 1 kHz frequency.

(C) Correlation of the maximal failure-free AP frequency and the AP half-duration recorded in n = 10 mossy fibers (Pearson's correlation coefficient $R = -0.71$; $p = 0.02$).

(D) Maximum failure-free frequency plotted versus stimulation frequency (top). The black bar shows the mean ± SEM (n = 10); colors indicate individual experiments. Corresponding half-duration (middle) and amplitude (bottom) of the last AP in the train normalized to the first AP.

(Figure 7B). Whereas capacitance measurements sample the total release from the entire cMFB, deconvolution based on the postsynaptic current from a GC samples only the fraction of total release of the cMFB that is directed toward the single GC recorded from (see illustration in Figure 7A). Therefore, quantitative comparison of the number of released vesicles with both techniques results in an estimate of the number of postsynaptic GCs per cMFB for each cMFB-GC pair. Assuming a single vesicle capacitance of 70 aF, the comparison revealed on average 100 ± 10 GCs per cMFB (Figure 7C, n = 10 cell pairs). This is higher than previous estimates (~10, Billings et al., 2014; ~50, Jakab and Hámori, 1988), but, e.g., a bias towards larger terminals, ectopic vesicle release, postsynaptic rundown, or release onto Golgi cells would lead to an overestimation of the connectivity ratio. Thus, we established two independent techniques with high temporal resolution, which allowed us to measure release at cMFBs directly.

Ultrafast Vesicle Recruitment and Tight Ca^{2+} Channel-Vesicle Coupling

Next we determined the number of release-ready vesicles, a central parameter to understanding the mechanisms of high-frequency synaptic transmission (Hallermann and Silver, 2013; Neher, 2010). The release rate based on deconvolution techniques showed an initial peak and a subsequent sustained part (cf. Figure 7A). The first peak most likely reflects fusion of release-ready vesicles, whereas the sustained part reflects vesicle recruitment (Sakaba and Neher, 2001b). Analysis of the cumulative release rates (Figure 8A) revealed that the initial release was best described by two exponential components with time constants of 0.43 ± 0.05 and 5.6 ± 1.4 ms (consisting of N_1 = 15.2 ± 4.3 and N_2 = 7.3 ± 1.4 vesicles; n = 10; Table S1). These estimates of the number of release-ready vesicles are slightly higher than estimates using extracellular stimulation techniques (5–10 vesicles; Saviane and Silver, 2006; Hallermann et al., 2010), but much smaller than estimates at the calyx of Held (range 700–5,000; Borst and Soria van Hoeve, 2012). The sustained part was well described by a line with an average slope of 358 ± 132 vesicles · s^{-1} (n = 10; Figure 8A; Table S1). These data indicate two populations of release-ready vesicles and a rapid recruitment speed of ~350 vesicles · s^{-1}, which can be sustained for up to 100 ms.

To analyze the coupling distance of vesicles to Ca^{2+} channels, we substantially increased the intrabouton Ca^{2+} buffering by raising the concentration of the slow Ca^{2+} buffer EGTA in the presynaptic solution from our control value of 200 µM to 5 mM. The time constant and the amplitude of the first component of release were not significantly changed by 5 mM EGTA ($p = 0.42$ and 0.96, respectively, Mann-Whitney U test; Figure 8A), which indicates that these vesicles are tightly coupled to Ca^{2+} channels. However, including 5 mM EGTA in the presynaptic pipette resulted in a decrease of the slowly releasing

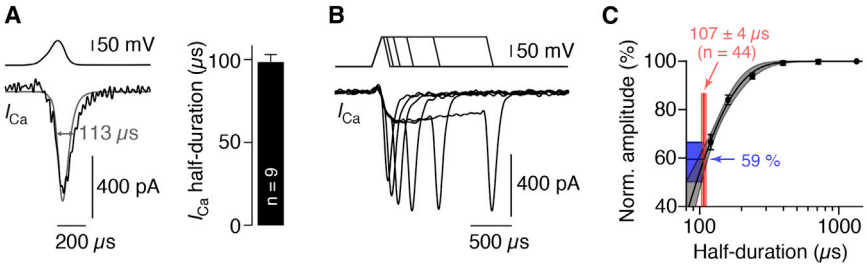

Figure 5. Efficient Opening of Ca^{2+} Channels during cMFB APs

(A) Left: Pharmacologically isolated Ca^{2+} current (I_{Ca}, bottom) evoked by an AP voltage command recorded in a cMFB (top) superimposed with the prediction of a m^2 Hodgkin-Huxley model calculated with the AP-voltage command. The half-duration of the measured current is indicated. Right: Average half-duration of the measured Ca^{2+} current (mean ± SEM; n represents number of cMFBs).

(B) Pharmacologically isolated Ca^{2+} current evoked by AP-like voltage commands of different half-durations (120, 160, 240, 400, 720, 1,360 μs).

(C) Peak amplitudes of Ca^{2+} currents evoked by AP-like voltage commands. Data (means ± SEM, n = 10) were normalized to the maximum value of each experiment and fit with a monoexponential function (black line). Superposition of the 95% confidence band of the fit (gray) with the average AP half-duration (104 ± 7 μs, n = 44; red) results in an estimate of relative Ca^{2+} channel open probability during an AP of 59% with a range of 50%–66% (blue; see also Figure S4).

component (N_2, $p < 0.01$, Mann-Whitney U test; Figure 8A), suggesting that these vesicles are remote from Ca^{2+} channels (Wadel et al., 2007) or that they have a lower intrinsic Ca^{2+} affinity (Lee et al., 2013; Wölfel et al., 2007). The slope of the linear part of the fits was not reduced with 5 mM EGTA ($p = 0.11$, Mann-Whitney U test; Figure 8A), indicating that EGTA does not block recruitment of vesicles to the release site. We further analyzed the kinetics of release with capacitance measurements. As with deconvolution techniques, two components of release and a linear vesicle recruitment rate were observed. The second release component was blocked by 5 mM EGTA, but the slope of the linear component was unaffected (Figure 8B; Table S1).

To relate these parameters to release evoked by AP trains, we recorded EPSCs in GCs elicited by extracellular stimulation of mossy fibers at 300 Hz (Figure 8C). We analyzed the number of release-ready vesicles and the vesicle recruitment rate by back-extrapolation of the cumulative EPSC amplitude (Figure 8D; Schneggenburger et al., 1999; Thanawala and Regehr, 2013). This analysis revealed 13.7 ± 3.4 release-ready vesicles and a recruitment rate of 469 ± 150 s^{-1} (n = 10), consistent with previous estimates at this synapse (Saviane and Silver, 2006; Hallermann et al., 2010). Interestingly, the values are similar to N_1 and s determined with prolonged depolarizations (cf. Figure 8A). This indicates that fast-releasing (N_1) but not slow-releasing vesicles (N_2) contribute to AP-evoked release (Sakaba, 2006) and that the maximal vesicle recruitment rate is similar during AP trains and prolonged presynaptic voltage steps. Furthermore, application of the membrane-permeable Ca^{2+} chelator EGTA-AM (100 μM) reduced the EPSC amplitude by 37% ($p < 0.01$, Wilcoxon signed-rank test; Figure 8C). Since 100 μM EGTA-AM was continuously applied at physiological temperatures, the intracellular EGTA concentration could be much higher than 5 mM. Therefore, no conclusions about the coupling distance can be drawn from these experiments. In contrast, the rate of vesicle recruitment was not significantly changed upon EGTA-AM application ($p = 0.77$, Wilcoxon signed-rank test; Figure 8D), which is again consistent with the lack of effect of 5 mM EGTA on the vesicle recruitment rate during depolarizations (cf. Figure 8A). In order to relate the recruitment rate to the vesicles that contribute to AP-evoked release, we divided the recruitment rate by the number of fast-releasing vesicles that mediate AP-evoked release. This resulted in a recruitment rate of 24 s^{-1} with prolonged depolarization using deconvolution, 50 s^{-1} with prolonged depolarization using capacitance measurements, and 34 s^{-1} with train stimulation using back-extrapolation (Table S1). Thus, deconvolution technique, capacitance measurements, and train stimulation revealed a small pool of release-ready vesicles, containing vesicles tightly coupled to Ca^{2+} channels, and rapid vesicle recruitment that can be sustained for > 100 ms.

DISCUSSION

In this study, paired recordings between cMFBs and GC allowed us to analyze the mechanisms of high-frequency signaling at highly divergent presynaptic boutons transmitting onto dozens of postsynaptic partners (Jörntell and Ekerot, 2006; Rancz et al., 2007; Saviane and Silver, 2006). We identified a unique set of presynaptic properties enabling single cMFB-GC connections to sustain kHz transmission during short bursts of APs: ultrafast, metabolically efficient APs can occur at bursts of up to 1.5 kHz, $Ca_v2.1$ Ca^{2+} channels open efficiently during APs, a subset of vesicles is tightly coupled to Ca^{2+} channels, and vesicles are rapidly recruited to the release site. Thus, our results establish a set of parameters enabling central synapses to operate in the kHz range.

Ultrafast APs

The AP is the basal unit for neuronal information processing, and its duration represents an ultimate limit for the maximal firing frequency. We recorded APs in cMFBs with ~100 μs half-duration (Figure 2). All previously measured AP half-durations are at least 2-fold longer. This is surprising because the AP shape has been studied extensively at a large number of cell types, including cells that transmit high-frequency signals (Borst and Sakmann, 1998; Rancz et al., 2007; Sabatini and Regehr, 1996). At cMFBs, previous estimates of AP half-duration in rats at physiological temperature (Rancz et al., 2007) and in turtles at room temperature (Thomsen et al., 2010) were several-fold longer; however, species differences and different recording conditions may account for this discrepancy. Yet extracellular recordings from cats in vivo are consistent with 100 μs half-durations of APs in cMFBs (Garwicz et al., 1998). Furthermore, a half-duration of ~100 μs is expected for the mature calyx of Held at physiological

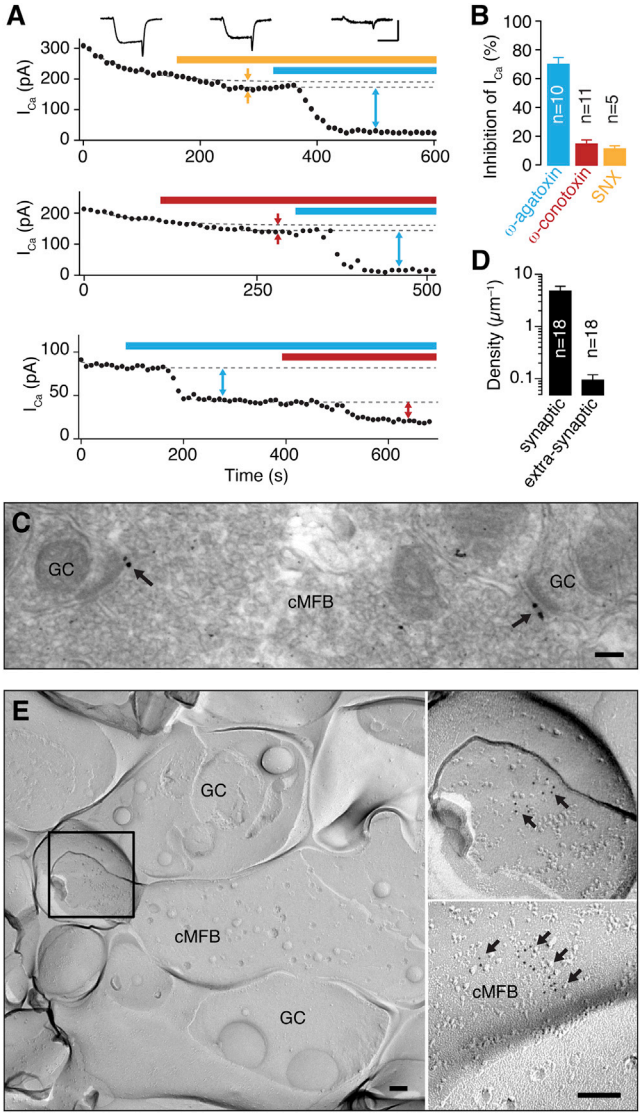

Figure 6. $Ca_V2.1$ Ca^{2+} Channels at Active Zones of cMFBs

(A) Steady-state amplitude of Ca^{2+} currents evoked by 3 ms depolarizations to 0 mV before and during application of 0.5 μM SNX-482 and 0.5 μM ω-Agatoxin (top), 1 μM ω-Conotoxin and 0.5 μM ω-Agatoxin (middle), or 0.5 μM ω-Agatoxin and 1 μM ω-Conotoxin (bottom). Horizontal bars indicate time of toxin application and dashed lines represent single exponential fits to the initial part of Ca^{2+} current amplitudes to account for rundown. Inset: Example Ca^{2+} currents for the first shown experiment before (left trace) and after wash-in of the toxins (middle and right traces). Scale bars, 200 pA and 2 ms.

(B) Average inhibition of Ca^{2+} currents by 0.5 μM ω-Agatoxin, 1 μM ω-Conotoxin, and 0.5 μM SNX-482 (mean ± SEM).

(C) Pre-embedding immunogold electron-microscopic labeling showing localization of $Ca_V2.1$ Ca^{2+} channels in the presynaptic active zones of a cMFB from a wild-type mouse. GC, granule cell dendrite. Arrows point toward gold particles. Scale bar, 100 nm.

(D) Average $Ca_V2.1$ immunogold density in cMFB profiles within and outside the active zones on a logarithmic scale (mean ± SEM).

(E) Freeze-fracture replica electron micrograph showing clusters of $Ca_V2.1$ Ca^{2+} channels in cMFBs from a 3-week-old mouse. Left: Low-magnification electron micrograph showing cross-fracture of a mossy fiber terminal (cMFB) with vesicles and continuous P-face of the same terminal contacting a granule cell dendrite (GC). A square part is enlarged (upper right) to show nine particles for $Ca_V2.1$ clustered at the active zone. Lower right: The picture derives from a different cMFB showing 17 particles. Arrows point toward gold particles. Scale bars, 100 nm.

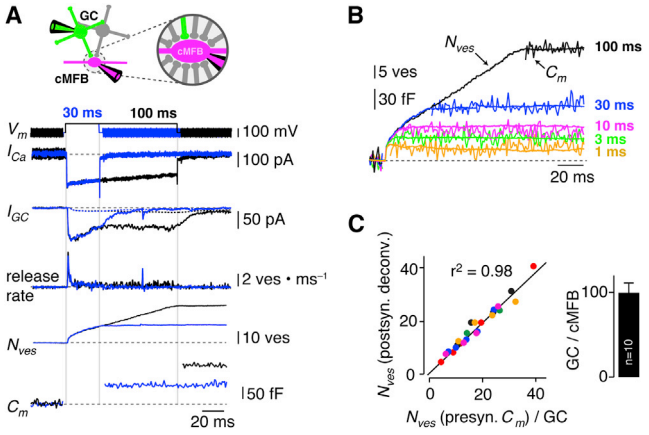

Figure 7. Measuring Vesicular Release Simultaneously from Presynaptic Capacitance Increase and Postsynaptic Currents

(A) Top: Illustration of the paired cMFB-GC recording configuration. The inset highlights the divergence of each cMFB contacting the GC recorded from (green) as well as many other GCs' dendrites (gray). Below: Example voltage command for cMFB (V_m), Ca^{2+} current in cMFB (I_{Ca}), EPSC in the GC (I_{GC}), deconvolved release rate, cumulative release rate (N_{ves}), and the capacitance increase in the cMFB (C_m) are plotted for a 30 ms (blue) and 100 ms (black) cMFB depolarization.

(B) Superposition of capacitance increase (C_m) in cMFB and cumulative release rate (N_{ves}) estimated by deconvolution of the postsynaptic GC EPSC for different pulse durations as indicated for the example experiment shown in (A).

(C) Left: Comparison of the presynaptic (C_m) and postsynaptic (deconvolution) estimates of the number of released vesicles per MF-GC connection. Each color represents a paired cMFB-GC recording with duration of depolarizations ranging from 1 to 100 ms. Right: Resulting average number of GC per cMFB based on n = 10 paired recordings (mean ± SEM).

temperature (Taschenberger and von Gersdorff, 2000), although such recordings have not been performed, and previously measured values at the immature calyx or at room temperatures were > 200 μs (Borst and Sakmann, 1998; Taschenberger and von Gersdorff, 2000; Yang and Wang, 2006). In general, fast-spiking neurons seem to have APs with short duration (Carter and Bean, 2009). Accordingly, maximal firing frequency and AP half-duration were correlated within the here-analyzed population of cMFBs (Figure 4C). Similar results have been obtained at two classes of vestibular nucleus neurons (Gittis et al., 2010). The very short half-duration of APs in cMFBs likely represents a special adaptation to the high frequencies that these presynaptic terminals operate at (Figure 4; Rancz et al., 2007).

To get an insight into the underlying mechanisms, we analyzed the properties of Na^+ and K^+ channels. Our estimated Na^+ current density was similar to the density at axons of hippocampal interneurons (Hu and Jonas, 2014). Furthermore, Na^+ channels were rapidly inactivating, resulting in a Na^+ excess ratio of ~1.8 (Figure 3), which is similar to the axon initial segment of layer 5 pyramidal cells (Hallermann et al., 2012) and slightly larger

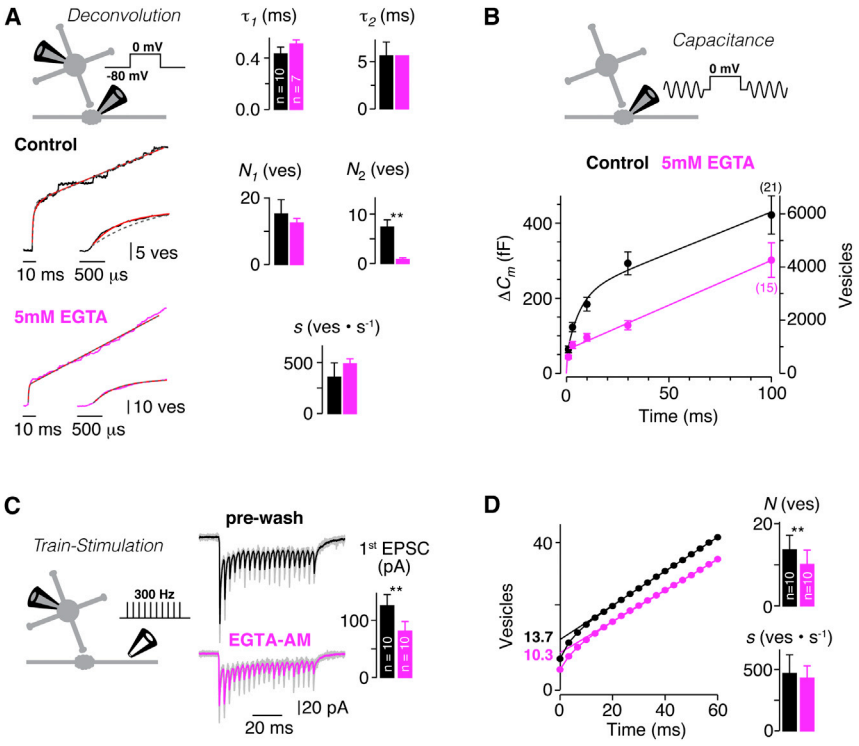

Figure 8. Ultrafast Vesicle Recruitment and Tight Ca^{2+} Channel-Vesicle Coupling

(A) Left: Example of cumulative release rates during a 100 ms depolarization in control (black; presynaptic pipette contained 200 µM EGTA) and with increased Ca^{2+} buffering in the cMFB (magenta; 5 mM EGTA) superimposed with a fit consisting of the sum of a biexponential function and a line (red) and the sum of a monoexponential function and a line (dashed gray). Inset: Initial cumulative release rate on an expanded timescale. Right: Average fit parameters of the sum of a biexponential function and a line for control (black) and high-EGTA conditions (magenta; mean ± SEM; n represents the number of paired cMFB-GC recordings). For 5 mM EGTA, τ_2 was fixed to the control value.

(B) Average capacitance increases (ΔC_m) plotted versus the length of the depolarizing pulse in control condition (black; n = 21) and with 5 mM EGTA (magenta; mean ± SEM; n = 15; n represents the number of cMFB recordings). The right axis indicates the number of vesicles based on 70 aF/vesicle. See Table S1 for parameters of the fits.

(C) Left: Example EPSCs (gray) evoked by 300 Hz axonal stimulation (20 stimuli; recording configuration depicted by the inset) recorded in a cMFB superimposed with the corresponding average before (black) and after bath application of 100 µM EGTA-AM (magenta). Right: Average amplitude of the first EPSC for control and EGTA-AM (black and magenta, respectively; mean ± SEM; n = 10).

(D) Left: Average cumulative number of released vesicles before (black) and after application of EGTA-AM (magenta). The estimated number of release-ready vesicles by back-extrapolation is indicated. Right: Average number of release-ready vesicles (*N*) and slope (*s*) estimated from the back-extrapolation of individual experiments before and after application of EGTA-AM (mean ± SEM; see also Table S1).

than at hippocampal mossy fiber boutons (Alle et al., 2009). The AP efficiency is surprising because short half-durations of APs tend to come at a cost of metabolic inefficiency (Carter and Bean, 2009, 2011).

The repolarization of cMFB APs was mediated by both K_{v1} and K_{v3} channels (Figure 2). This is in contrast to findings at the Purkinje cell soma, the boutons of cerebellar interneuron axons, or the calyx of Held, where K_{v3} dominates the repolarization (Ishikawa et al., 2003; Martina et al., 2007; Rowan et al., 2014; Wang et al., 1998). However, both K_{v1} and K_{v3} channels cause the repolarization of hippocampal mossy fiber boutons (Alle et al., 2011). The speed of K^+ channel activation measured here at cMFBs was fast, but comparable to K^+ channel activation kinetics measured previously (Alle et al., 2011; Martina et al., 2007), indicating that the ultrafast APs at cMFBs cannot be explained by rapid activation kinetics alone. Indeed, our Hodgkin-Huxley modeling based on measured gating kinetics predicted a high density of K^+ channels at cMFBs (Figure S3). However, in most outside-out patches from cMFBs, the estimated K^+ current density was low. This discrepancy is consistent with electron microscopic analysis showing that K_{v1} channels are highly clustered at fine protuberances of cMFBs, making density estimates from outside-out patches unreliable (Figure S3E; McNamara et al., 1996). In addition, cMFBs and the adjacent myelinated axons have structural similarities with nodes of Ranvier (Palay and Chan-Palay, 1974), suggesting that K^+ channels are clustered at the adjacent mossy fiber axon comparable to the K^+ channel clustering observed at juxtaparanodal zones of the nodes of Ranvier (Rasband and Shrager, 2000). Thus, although we have no direct experimental evidence, our results suggest a high density of inhomogeneously distributed K^+ channels. Furthermore, our data indicate a high density of rapidly gating Na^+ channels underlying ultrafast but metabolically efficient APs at cMFBs.

Presynaptic Ca^{2+} Currents

The exceptionally short duration of cMFB APs raised the question how Ca^{2+} channels are recruited during APs. In principle, reliable synaptic transmission can be obtained either by efficient opening of few presynaptic Ca^{2+} channels during APs (as shown, e.g., at the calyx of Held; Borst and Sakmann, 1998; but see also Sheng et al., 2012) or by inefficient opening of many Ca^{2+} channels (as shown, e.g., at the neuromuscular junction; Luo et al., 2011). Our analysis indicates efficient Ca^{2+} channel opening despite the short duration of APs (Figure 5). This implies that activation kinetics of Ca^{2+} channels is very fast. Indeed, experiments with step-like depolarizations revealed activation kinetics of < 100 µs at 0 mV (Figure S4). This is more than 5-fold faster than previous estimates at central synapses at room temperature (Borst and Sakmann, 1998; Li et al., 2007; Lin et al., 2011) and is consistent with a strong temperature dependence of Ca^{2+} channel kinetics (Sabatini and Regehr, 1996). Furthermore, a Hodgkin-Huxley-type model of Ca^{2+} channels based on the measured activation and inactivation kinetics predicted efficient

channel opening. To gain insight into the molecular mechanism of fast Ca^{2+} channel gating, we determined the contribution of the different Ca^{2+} channel subtypes at cMFBs. Electrophysiological recordings showed that $Ca_v2.1$ Ca^{2+} channels contribute ~70% of the total Ca^{2+} current in cMFBs (Figure 6B). Furthermore, pre-embedding immunogold and freeze-fracture replica labeling indicated clustering of $Ca_v2.1$ Ca^{2+} channels at the active zone (Figures 6C and 6D). Thus, rapidly activating $Ca_v2.1$ Ca^{2+} channels ensure efficient calcium influx at the active zone during fast cMFB APs.

Tight Vesicle to Ca^{2+} Channel Coupling

The first component of release was not significantly slowed by 5 mM EGTA in cMFB (Figure 8A). In contrast, at the immature calyx of Held synapse, 5 mM EGTA prolonged the first component of release (Sakaba and Neher, 2001a). Thus, compared with loose vesicle to Ca^{2+} channel coupling at the immature calyx (Meinrenken et al., 2002), the mature cMFBs studied here display tight vesicle to Ca^{2+} channel coupling. Tight coupling has been observed at many synapses mediating high frequency synaptic transmission, such as the mature calyx of Held (Wang et al., 2008), the hippocampal basket cell to granule cell synapse (Bucurenciu et al., 2008), and the parallel fiber to Purkinje cell synapse (Schmidt et al., 2013). On the other hand, the mature hippocampal mossy fiber to CA3 pyramidal cell synapse exhibits loose coupling (Vyleta and Jonas, 2014). The tight and loose vesicle to Ca^{2+} channel coupling in cerebellar and hippocampal mossy fiber boutons, respectively, seems consistent with their markedly different function within the corresponding neuronal network (Delvendahl et al., 2013).

Vesicle Recruitment Rate

We found a vesicle recruitment rate of ~400 vesicles • s^{-1} during 100 ms depolarizations and during high-frequency synaptic transmission for each cMFB-GC connection at physiological temperatures (Figure 8). For the entire cMFB, the rate was 30,000 vesicles • s^{-1} (Figure 8B). At the calyx of Held synapse, at which vesicle recruitment has been intensely studied, a value of less than 10,000 vesicles • s^{-1} has been estimated at room temperature (Neher, 2010; Sakaba and Neher, 2001b; Wölfel et al., 2007), but higher values have also been obtained (100,000 and 170,000 vesicles • s^{-1}, at room and physiological temperatures; based on 7,500 and 12,300 fF/s, respectively; Kushmerick et al., 2006). Relating the vesicle recruitment rate to the number of fast-releasing vesicles in cMFBs resulted in estimates ranging from 24 to 50 s^{-1} (Figure 8). This is lower than previous estimates based on postsynaptic techniques at cMFBs (~70 s^{-1}; Saviane and Silver, 2006; Hallermann et al., 2010), but higher than estimates at the calyx of Held (~11 s^{-1}; physiological temperature; Kushmerick et al., 2006). High rates of vesicle recruitment have also been observed at cerebellar parallel fibers (Crowley et al., 2007; Valera et al., 2012; but see van Beugen et al., 2013). Thus, vesicle recruitment at cMFBs is remarkably fast.

Limited Surface Area at a Highly Divergent Synapse

One obvious explanation for the high vesicle recruitment rate in cMFBs could reside in the fact that each cMFB contacts more than 10 dendrites of GCs (Billings et al., 2014; Jakab and Hámori, 1988; Figure 7C). This limits the surface area that is available for each postsynaptic partner. The limited number of release sites must therefore rely on rapid vesicle recruitment (Saviane and Silver, 2006). Consistently, the cMFB-GC synapse has been described as a "device to secure a high mossy fiber to GC divergence with minimal physical structure" (Eccles et al., 1967). In contrast, large synapses with 1:1 connectivity, such as the neuromuscular junction (Luo et al., 2011), the Purkinje cell to cerebellar nuclear neuron synapse (Telgkamp et al., 2004), the hippocampal mossy fiber to CA3 pyramidal neuron synapse (Hallermann et al., 2003), the vestibular afferent synapse (Bagnall et al., 2008), and the endbulb of Held synapse (Lin et al., 2011), rely on a large pool of release-ready vesicles with low release probabilities. Therefore, these 1:1 synapses can sustain efficient release by the parallel usage of many release sites despite slow vesicle recruitment at each site, whereas cMFB-GC synapses sustain efficient release with fewer release sites and rapid vesicle recruitment (cf. Box 1 in Hallermann and Silver, 2013). Thus, the limited space for synaptic contact at the cMFB-GC synapse might provide an explanation for the rapid vesicle recruitment.

Implications for Information Processing

To control timing (Ivry and Keele, 1989), the cerebellar cortex relies on high-frequency firing of mossy fibers (Garwicz et al., 1998; Rancz et al., 2007), granule cells (Jörntell and Ekerot, 2006), and Purkinje cells (Blot and Barbour, 2014; Thach, 1972). Quantitative comparison of these data suggests that the frequency of a signal is highest in mossy fibers and gradually becomes lower during propagation through granule and Purkinje cells. Interestingly, GCs may linearly encode the strength of cMFB firing (Chadderton et al., 2004; Gabbiani et al., 1994). Linear processing also occurs at parallel fiber to Purkinje cell transmission, but in a lower frequency range (Walter and Khodakhah, 2006). The frequency reduction and the linear processing suggest that the cerebellar cortex receives mossy fiber input in the kHz range (Rancz et al., 2007; Figure 4), performs additive and (via gain modulation) multiplicative scaling of rate-coded inputs (Silver, 2010), and provides an output at frequencies still high but lower than the input. Thereby, computation at exceptionally fast timescales can be achieved. Future studies will have to analyze the advantages of high-frequency firing of individual neurons, in particular in consideration of the fact that other brain regions, such as the visual system, can process information rapidly, even though the firing rates of the individual neurons are much lower (Rieke et al., 1997; Tchumatchenko et al., 2011).

In summary, by using paired recordings between cMFBs and GCs in combination with high-resolution techniques, we were able to directly measure fundamental parameters that enable high-frequency synaptic transmission. Our study provides insight into the exceptionally diverse repertoire of synaptic functions at central synapses.

EXPERIMENTAL PROCEDURES

Methods are described in detail in the Supplemental Experimental Procedures.

Presynaptic Recordings from cMFBs

Recordings were performed in acute sagittal cerebellar slices from mature (>P20) TgN(Thy1-EYFP) (Hirrlinger et al., 2005) or C57BL/6 mice at 35°C – 37°C. To increase the success rate of presynaptic recordings from cMFBs, two-photon guided patch-clamp recordings (Margrie et al., 2003) were performed in the TgN(Thy1-EYFP)-mice with a Femto-2D two-photon microscope (Femtonics, Budapest) and a 60x Olympus (NA 1.0) objective. Alternatively, cMFBs were identified with infrared differential interference contrast (DIC) optics using a FN-1 microscope from Nikon with a 100x objective (NA 1.1). All current-clamp and voltage-clamp recordings from cMFBs and GCs were performed with an EPC10/2 amplifier (HEKA Elektronik, Lambrecht/Pfalz).

Identification of cMFB Recordings

To unequivocally identify cMFBs, two alternative methods were used: (1) in presynaptic recordings with potassium-based intracellular solutions, the distinctive electrical properties including pronounced outward rectification and time-dependent "sag" of membrane potential on hyperpolarization were used (Rancz et al., 2007); (2) in presynaptic recordings with cesium-based intracellular solutions (and TTX in the bath), the capacitance increase upon depolarization confirmed the identity of cMFBs, since other cells such as GCs did not show capacitance increases (if any, < 20 fF). In addition, Atto 594 in the presynaptic intracellular solution allowed visualizing the mossy fiber axon.

Paired Recordings between cMFBs and GC

For paired pre- and postsynaptic recordings, GCs were whole-cell patch-clamped with intracellular solution containing 100 μM Atto 594 or Atto 488, and cMFBs near dendrites were identified by their EYFP expression in TgN(Thy1-EYFP) mice or by differential interference contrast microscopy. The reliable induction of an EPSC in the GC upon depolarization of the presynaptic structure was used to unequivocally identify a cMFB.

SUPPLEMENTAL INFORMATION

Supplemental Information includes Supplemental Experimental Procedures, four figures, and one table and can be found with this article online at http://dx.doi.org/10.1016/j.neuron.2014.08.036.

ACKNOWLEDGMENTS

We would like to thank Erwin Neher for helpful discussions and for advice during the implementation of the deconvolution of postsynaptic currents; Erwin Neher, Maarten Kole, and Manfred Heckmann for critically reading the manuscript; Masahiko Watanabe for providing $Ca_v2.1$ antibody; and Walter Kaufmann for technical assistance. This work was supported by the Heisenberg Program of the German Research Foundation to S.H. (HA 6386/1-1, 2-1, and 3-1) and by the German Research Foundation to J.H. (HI1414/2-1) and partly funded by the Wellcome Trust (ref: 097829) through the Centre for Chronic Diseases and Disorders (C2D2) at the University of York.

Accepted: August 17, 2014
Published: September 11, 2014

REFERENCES

Alle, H., Roth, A., and Geiger, J.R.P. (2009). Energy-efficient action potentials in hippocampal mossy fibers. Science *325*, 1405–1408.

Alle, H., Kubota, H., and Geiger, J.R. (2011). Sparse but highly efficient K_v3 outpace BK_{Ca} channels in action potential repolarization at hippocampal mossy fiber boutons. J. Neurosci. *31*, 8001–8012.

Arenz, A., Silver, R.A., Schaefer, A.T., and Margrie, T.W. (2008). The contribution of single synapses to sensory representation in vivo. Science *321*, 977–980.

Bagnall, M.W., McElvain, L.E., Faulstich, M., and du Lac, S. (2008). Frequency-independent synaptic transmission supports a linear vestibular behavior. Neuron *60*, 343–352.

Bean, B.P. (2007). The action potential in mammalian central neurons. Nat. Rev. Neurosci. *8*, 451–465.

Billings, G., Piasini, E., Lőrincz, A., Nusser, Z., and Silver, R.A. (2014). Network structure within the cerebellar input layer enables lossless sparse encoding. Neuron *83*, 960–974.

Blot, A., and Barbour, B. (2014). Ultra-rapid axon-axon ephaptic inhibition of cerebellar Purkinje cells by the pinceau. Nat. Neurosci. *17*, 289–295.

Borst, J.G., and Sakmann, B. (1998). Calcium current during a single action potential in a large presynaptic terminal of the rat brainstem. J. Physiol. *506*, 143–157.

Borst, J.G., and Soria van Hoeve, J. (2012). The calyx of held synapse: from model synapse to auditory relay. Annu. Rev. Physiol. *74*, 199–224.

Bucurenciu, I., Kulik, A., Schwaller, B., Frotscher, M., and Jonas, P. (2008). Nanodomain coupling between Ca^{2+} channels and Ca^{2+} sensors promotes fast and efficient transmitter release at a cortical GABAergic synapse. Neuron *57*, 536–545.

Carter, B.C., and Bean, B.P. (2009). Sodium entry during action potentials of mammalian neurons: incomplete inactivation and reduced metabolic efficiency in fast-spiking neurons. Neuron *64*, 898–909.

Carter, B.C., and Bean, B.P. (2011). Incomplete inactivation and rapid recovery of voltage-dependent sodium channels during high-frequency firing in cerebellar Purkinje neurons. J. Neurophysiol. *105*, 860–871.

Chadderton, P., Margrie, T.W., and Häusser, M. (2004). Integration of quanta in cerebellar granule cells during sensory processing. Nature *428*, 856–860.

Crowley, J.J., Carter, A.G., and Regehr, W.G. (2007). Fast vesicle replenishment and rapid recovery from desensitization at a single synaptic release site. J. Neurosci. *27*, 5448–5460.

Delvendahl, I., Weyhersmüller, A., Ritzau-Jost, A., and Hallermann, S. (2013). Hippocampal and cerebellar mossy fibre boutons - same name, different function. J. Physiol. *591*, 3179–3188.

DiGregorio, D.A., Nusser, Z., and Silver, R.A. (2002). Spillover of glutamate onto synaptic AMPA receptors enhances fast transmission at a cerebellar synapse. Neuron *35*, 521–533.

Eccles, J.C., Ito, M., and Szentagothai, J. (1967). The Cerebellum as a Neuronal Machine. (Berlin: Springer-Verlag).

Gabbiani, F., Midtgaard, J., and Knöpfel, T. (1994). Synaptic integration in a model of cerebellar granule cells. J. Neurophysiol. *72*, 999–1009.

Garwicz, M., Jörntell, H., and Ekerot, C.F. (1998). Cutaneous receptive fields and topography of mossy fibres and climbing fibres projecting to cat cerebellar C3 zone. J. Physiol. *512*, 277–293.

Geiger, J.R.P., and Jonas, P. (2000). Dynamic control of presynaptic Ca^{2+} inflow by fast-inactivating K^+ channels in hippocampal mossy fiber boutons. Neuron *28*, 927–939.

Gittis, A.H., Moghadam, S.H., and du Lac, S. (2010). Mechanisms of sustained high firing rates in two classes of vestibular nucleus neurons: differential contributions of resurgent Na, Kv3, and BK currents. J. Neurophysiol. *104*, 1625–1634.

Gutman, G.A., Chandy, K.G., Grissmer, S., Lazdunski, M., McKinnon, D., Pardo, L.A., Robertson, G.A., Rudy, B., Sanguinetti, M.C., Stühmer, W., and Wang, X. (2005). International Union of Pharmacology. LIII. Nomenclature and molecular relationships of voltage-gated potassium channels. Pharmacol. Rev. *57*, 473–508.

Hallermann, S., and Silver, R.A. (2013). Sustaining rapid vesicular release at active zones: potential roles for vesicle tethering. Trends Neurosci. *36*, 185–194.

Hallermann, S., Pawlu, C., Jonas, P., and Heckmann, M. (2003). A large pool of releasable vesicles in a cortical glutamatergic synapse. Proc. Natl. Acad. Sci. USA *100*, 8975–8980.

Hallermann, S., Fejtova, A., Schmidt, H., Weyhersmüller, A., Silver, R.A., Gundelfinger, E.D., and Eilers, J. (2010). Bassoon speeds vesicle reloading at a central excitatory synapse. Neuron *68*, 710–723.

Hallermann, S., de Kock, C.P., Stuart, G.J., and Kole, M.H. (2012). State and location dependence of action potential metabolic cost in cortical pyramidal neurons. Nat. Neurosci. *15*, 1007–1014.

Hirrlinger, P.G., Scheller, A., Braun, C., Quintela-Schneider, M., Fuss, B., Hirrlinger, J., and Kirchhoff, F. (2005). Expression of reef coral fluorescent proteins in the central nervous system of transgenic mice. Mol. Cell. Neurosci. *30*, 291–303.

Hu, H., and Jonas, P. (2014). A supercritical density of Na^+ channels ensures fast signaling in GABAergic interneuron axons. Nat. Neurosci. *17*, 686–693.

Indriati, D.W., Kamasawa, N., Matsui, K., Meredith, A.L., Watanabe, M., and Shigemoto, R. (2013). Quantitative localization of $Ca_v2.1$ (P/Q-type) voltage-dependent calcium channels in Purkinje cells: somatodendritic gradient and distinct somatic coclustering with calcium-activated potassium channels. J. Neurosci. *33*, 3668–3678.

Ishikawa, T., Nakamura, Y., Saitoh, N., Li, W.B., Iwasaki, S., and Takahashi, T. (2003). Distinct roles of Kv1 and Kv3 potassium channels at the calyx of Held presynaptic terminal. J. Neurosci. *23*, 10445–10453.

Ivry, R.B., and Keele, S.W. (1989). Timing functions of the cerebellum. J. Cogn. Neurosci. *1*, 136–152.

Jakab, R.L., and Hámori, J. (1988). Quantitative morphology and synaptology of cerebellar glomeruli in the rat. Anat. Embryol. (Berl.) *179*, 81–88.

Jörntell, H., and Ekerot, C.F. (2006). Properties of somatosensory synaptic integration in cerebellar granule cells *in vivo*. J. Neurosci. *26*, 11786–11797.

Kushmerick, C., Renden, R., and von Gersdorff, H. (2006). Physiological temperatures reduce the rate of vesicle pool depletion and short-term depression via an acceleration of vesicle recruitment. J. Neurosci. *26*, 1366–1377.

Leão, R.M., Kushmerick, C., Pinaud, R., Renden, R., Li, G.L., Taschenberger, H., Spirou, G., Levinson, S.R., and von Gersdorff, H. (2005). Presynaptic Na^+ channels: locus, development, and recovery from inactivation at a high-fidelity synapse. J. Neurosci. *25*, 3724–3738.

Lee, J.S., Ho, W.K., Neher, E., and Lee, S.H. (2013). Superpriming of synaptic vesicles after their recruitment to the readily releasable pool. Proc. Natl. Acad. Sci. USA *110*, 15079–15084.

Li, L., Bischofberger, J., and Jonas, P. (2007). Differential gating and recruitment of P/Q-, N-, and R-type Ca^{2+} channels in hippocampal mossy fiber boutons. J. Neurosci. *27*, 13420–13429.

Lien, C.C., and Jonas, P. (2003). Kv3 potassium conductance is necessary and kinetically optimized for high-frequency action potential generation in hippocampal interneurons. J. Neurosci. *23*, 2058–2068.

Lin, K.H., Oleskevich, S., and Taschenberger, H. (2011). Presynaptic Ca^{2+} influx and vesicle exocytosis at the mouse endbulb of Held: a comparison of two auditory nerve terminals. J. Physiol. *589*, 4301–4320.

Liu, P.W., and Bean, B.P. (2014). Kv2 channel regulation of action potential repolarization and firing patterns in superior cervical ganglion neurons and hippocampal CA1 pyramidal neurons. J. Neurosci. *34*, 4991–5002.

London, M., Roth, A., Beeren, L., Häusser, M., and Latham, P.E. (2010). Sensitivity to perturbations *in vivo* implies high noise and suggests rate coding in cortex. Nature *466*, 123–127.

Luo, F., Dittrich, M., Stiles, J.R., and Meriney, S.D. (2011). Single-pixel optical fluctuation analysis of calcium channel function in active zones of motor nerve terminals. J. Neurosci. *31*, 11268–11281.

Margrie, T.W., Meyer, A.H., Caputi, A., Monyer, H., Hasan, M.T., Schaefer, A.T., Denk, W., and Brecht, M. (2003). Targeted whole-cell recordings in the mammalian brain in vivo. Neuron *39*, 911–918.

Martina, M., Metz, A.E., and Bean, B.P. (2007). Voltage-dependent potassium currents during fast spikes of rat cerebellar Purkinje neurons: inhibition by BDS-I toxin. J. Neurophysiol. *97*, 563–571.

McNamara, N.M., Averill, S., Wilkin, G.P., Dolly, J.O., and Priestley, J.V. (1996). Ultrastructural localization of a voltage-gated K^+ channel α subunit (K_V 1.2) in the rat cerebellum. Eur. J. Neurosci. *8*, 688–699.

Meinrenken, C.J., Borst, J.G., and Sakmann, B. (2002). Calcium secretion coupling at calyx of held governed by nonuniform channel-vesicle topography. J. Neurosci. *22*, 1648–1667.

Neher, E. (2010). What is rate-limiting during sustained synaptic activity: vesicle supply or the availability of release sites. Front Synaptic Neurosci *2*, 144, http://dx.doi.org/10.3389/fnsyn.2010.00144.

Palay, S.M., and Chan-Palay, V. (1974). Cerebellar Cortex: Cytology and Organization. (Berlin: Springer).

Rancz, E.A., Ishikawa, T., Duguid, I., Chadderton, P., Mahon, S., and Häusser, M. (2007). High-fidelity transmission of sensory information by single cerebellar mossy fibre boutons. Nature *450*, 1245–1248.

Rasband, M.N., and Shrager, P. (2000). Ion channel sequestration in central nervous system axons. J. Physiol. *525*, 63–73.

Rieke, F., Warland, D., de Ruyter van Steveninck, R.R., and Bialek, W. (1997). Spikes: Exploring the Neural Code. (Cambridge, Massachusetts: MIT Press).

Rowan, M.J.M., Tranquil, E., and Christie, J.M. (2014). Distinct K_v channel subtypes contribute to differences in spike signaling properties in the axon initial segment and presynaptic boutons of cerebellar interneurons. J. Neurosci. *34*, 6611–6623.

Rudy, B., and McBain, C.J. (2001). Kv3 channels: voltage-gated K^+ channels designed for high-frequency repetitive firing. Trends Neurosci. *24*, 517–526.

Sabatini, B.L., and Regehr, W.G. (1996). Timing of neurotransmission at fast synapses in the mammalian brain. Nature *384*, 170–172.

Sakaba, T. (2006). Roles of the fast-releasing and the slowly releasing vesicles in synaptic transmission at the calyx of held. J. Neurosci. *26*, 5863–5871.

Sakaba, T., and Neher, E. (2001a). Calmodulin mediates rapid recruitment of fast-releasing synaptic vesicles at a calyx-type synapse. Neuron *32*, 1119–1131.

Sakaba, T., and Neher, E. (2001b). Quantitative relationship between transmitter release and calcium current at the calyx of held synapse. J. Neurosci. *21*, 462–476.

Saviane, C., and Silver, R.A. (2006). Fast vesicle reloading and a large pool sustain high bandwidth transmission at a central synapse. Nature *439*, 983–987.

Schmidt, H., Brachtendorf, S., Arendt, O., Hallermann, S., Ishiyama, S., Bornschein, G., Gall, D., Schiffmann, S.N., Heckmann, M., and Eilers, J. (2013). Nanodomain coupling at an excitatory cortical synapse. Curr. Biol. *23*, 244–249.

Schneggenburger, R., Meyer, A.C., and Neher, E. (1999). Released fraction and total size of a pool of immediately available transmitter quanta at a calyx synapse. Neuron *23*, 399–409.

Sheng, M., Tsaur, M.L., Jan, Y.N., and Jan, L.Y. (1992). Subcellular segregation of two A-type K^+ channel proteins in rat central neurons. Neuron *9*, 271–284.

Sheng, J., He, L., Zheng, H., Xue, L., Luo, F., Shin, W., Sun, T., Kuner, T., Yue, D.T., and Wu, L.G. (2012). Calcium-channel number critically influences synaptic strength and plasticity at the active zone. Nat. Neurosci. *15*, 998–1006.

Silver, R.A. (2010). Neuronal arithmetic. Nat. Rev. Neurosci. *11*, 474–489.

Sun, J.Y., and Wu, L.G. (2001). Fast kinetics of exocytosis revealed by simultaneous measurements of presynaptic capacitance and postsynaptic currents at a central synapse. Neuron *30*, 171–182.

Taschenberger, H., and von Gersdorff, H. (2000). Fine-tuning an auditory synapse for speed and fidelity: developmental changes in presynaptic waveform, EPSC kinetics, and synaptic plasticity. J. Neurosci. *20*, 9162–9173.

Tchumatchenko, T., Malyshev, A., Wolf, F., and Volgushev, M. (2011). Ultrafast population encoding by cortical neurons. J. Neurosci. *31*, 12171–12179.

Telgkamp, P., Padgett, D.E., Ledoux, V.A., Woolley, C.S., and Raman, I.M. (2004). Maintenance of high-frequency transmission at purkinje to cerebellar nuclear synapses by spillover from boutons with multiple release sites. Neuron *41*, 113–126.

Thach, W.T. (1972). Cerebellar output: properties, synthesis and uses. Brain Res. *40*, 89–102.

Thanawala, M.S., and Regehr, W.G. (2013). Presynaptic calcium influx controls neurotransmitter release in part by regulating the effective size of the readily releasable pool. J. Neurosci. *33*, 4625–4633.

Thomsen, L.B., Jörntell, H., and Midtgaard, J. (2010). Presynaptic calcium signalling in cerebellar mossy fibres. Front Neural Circuits *4*, 1.

Valera, A.M., Doussau, F., Poulain, B., Barbour, B., and Isope, P. (2012). Adaptation of granule cell to Purkinje cell synapses to high-frequency transmission. J. Neurosci. *32*, 3267–3280.

van Beugen, B.J., Gao, Z., Boele, H.J., Hoebeek, F., and De Zeeuw, C.I. (2013). High frequency burst firing of granule cells ensures transmission at the parallel fiber to purkinje cell synapse at the cost of temporal coding. Front Neural Circuits *7*, 95.

von Gersdorff, H., Sakaba, T., Berglund, K., and Tachibana, M. (1998). Submillisecond kinetics of glutamate release from a sensory synapse. Neuron *21*, 1177–1188.

Vyleta, N.P., and Jonas, P. (2014). Loose coupling between Ca^{2+} channels and release sensors at a plastic hippocampal synapse. Science *343*, 665–670.

Wadel, K., Neher, E., and Sakaba, T. (2007). The coupling between synaptic vesicles and Ca^{2+} channels determines fast neurotransmitter release. Neuron *53*, 563–575.

Walter, J.T., and Khodakhah, K. (2006). The linear computational algorithm of cerebellar Purkinje cells. J. Neurosci. *26*, 12861–12872.

Wang, L.Y., and Kaczmarek, L.K. (1998). High-frequency firing helps replenish the readily releasable pool of synaptic vesicles. Nature *394*, 384–388.

Wang, L.Y., Gan, L., Forsythe, I.D., and Kaczmarek, L.K. (1998). Contribution of the Kv3.1 potassium channel to high-frequency firing in mouse auditory neurones. J. Physiol. *509*, 183–194.

Wang, L.Y., Neher, E., and Taschenberger, H. (2008). Synaptic vesicles in mature calyx of Held synapses sense higher nanodomain calcium concentrations during action potential-evoked glutamate release. J. Neurosci. *28*, 14450–14458.

Wölfel, M., Lou, X., and Schneggenburger, R. (2007). A mechanism intrinsic to the vesicle fusion machinery determines fast and slow transmitter release at a large CNS synapse. J. Neurosci. *27*, 3198–3210.

Yang, Y.M., and Wang, L.Y. (2006). Amplitude and kinetics of action potential-evoked Ca^{2+} current and its efficacy in triggering transmitter release at the developing calyx of held synapse. J. Neurosci. *26*, 5698–5708.